Published in final edited form as:
J Magn Reson Imaging. 2011 June ; 33(6): 1517–1525. doi:10.1002/jmri.22556.

Targeted Single-Shot Methods for Diffusion-Weighted Imaging in the Kidneys

Ning Jin, MS[1,2], **Jie Deng, PhD**[3], **Longjiang Zhang, MD**[4], **Zhuoli Zhang, MD, PhD**[2], **Guangming Lu, MD**[4], **Reed A. Omary, MD**[1,2,5], and **Andrew C. Larson, PhD**[1,2,5]

[1]Department of Biomedical Engineering, Northwestern University Chicago, Illinois, USA

[2]Department of Radiology, Northwestern University Chicago, Illinois, USA

[3]Depart of Medical Imaging Children's Memorial Hospital Chicago, Illinois, USA

[4]Department of Medical Imaging, Jinling Hospital, Clinical School of Medicine, Nanjing University, Nanjing, China

[5]Robert H. Lurie Comprehensive Cancer Center Chicago, Illinois, USA

Abstract

Purpose—To investigate the feasibility of combining the inner-volume-imaging (IVI) technique with single-shot diffusion-weighted (DW) spin-echo echo-planar imaging (SE-EPI) and DW-SPLICE (split acquisition of fast spin-echo) sequences for renal DW imaging.

Materials and Methods—Renal DW imaging was performed in 10 healthy volunteers using single-shot DW-SE-EPI, DW-SPLICE, targeted-DW-SE-EPI and targeted-DW-SPLICE. We compared the quantitative diffusion measurement accuracy and image quality of these targeted-DW-SE-EPI and targeted DW-SPLICE methods with conventional full FOV DW-SE-EPI and DW-SPLICE measurements in phantoms and normal volunteers.

Results—Compared with full FOV DW-SE-EPI and DW-SPLICE methods, targeted-DW-SE-EPI and targeted-DW-SPLICE approaches produced images of superior overall quality with fewer artifacts, less distortion and reduced spatial blurring in both phantom and volunteer studies. The ADC values measured with each of the four methods were similar and in agreement with previously published data. There were no statistically significant differences between the ADC values and intra-voxel incoherent motion (IVIM) measurements in the kidney cortex and medulla using single-shot DW-SE-EPI, targeted-DW-EPI and targeted-DW-SPLICE ($p > 0.05$).

Conclusion—Compared with full-FOV DW imaging methods, targeted-DW-SE-EPI and targeted-DW-SPLICE techniques reduced image distortion and artifacts observed in the single-shot DW-SE-EPI images, reduced blurring in DW-SPLICE images and produced comparable quantitative DW and IVIM measurements to those produced with conventional full-FOV approaches.

Keywords

renal; diffusion; targeted; inner volume imaging; SPLICE; EPI

Please send proof and correspondence to: Andrew C. Larson, Ph.D., NWU Radiology, 737 N. Michigan Ave Suite 1600, Chicago, IL 60611, USA, Tel: (312) 926-3499, a-larson@northwestern.edu.

INTRODUCTION

In vivo diffusion-weighted imaging (DWI) measurements are typically reflective of both the translational motion of water arising from molecular diffusion and microcirculation within capillary networks (perfusion) [1,2]. DWI techniques may prove particularly useful for non-invasive assessment of renal disease processes given the water transport function of the kidneys as well as the typically large blood flow rates through the kidneys. Several studies have recently used DWI methods to evaluate renal function in both native [3–5] and transplanted kidneys [6]; these DWI methods have also been useful for characterizing renal masses [7].

The single-shot DW spin-echo echo-planar imaging (DW-SE-EPI) approach is commonly employed during abdominal DWI studies because this sequence is generally insensitive to artifacts arising from bulk and physiologic motions. However, this technique can suffer from severe geometric distortion and artifacts due to susceptibility gradients and/or poor static field shimming [8]. The magnitude of these distortions and artifacts depends upon the field-of-view (FOV) and echo-train length (ETL). Alternative DW spin-echo based HASTE techniques, such as split acquisition of fast spin-echo signals for DWI (DW-SPLICE) [9], have been proposed. These techniques are resistant to field inhomogeneities, however, T2-filtering effects can commonly lead to image blurring in the phase-encoding (PE) direction, particularly when a long ETL is used. Hence, for both single-shot DW-SE-EPI and DW-SPLICE sequences, supplemental methods to reduce the ETL while preserving image resolution could be particularly helpful to improve overall image quality. Those methods include: parallel imaging (PI) [10,11], multi-shot image acquisition [12–14] and inner volume imaging (IVI) techniques [15,16].

PI acquisition, based on the combination of data acquired using a multi-element coil system, can be used to shorten ETL. However, the possible reduction in ETL depends on the coil geometry. Multi-shot image acquisitions, such as DW-PROPELLER[17] and multi-shot DW-SE-EPI [18], will increase image acquisition time significantly over conventional single-shot approaches. The inner volume image (IVI) technique, first proposed by Feinberg et al [19], involves selectively exciting a small region-of-interest (ROI) within the overall field-of-view (FOV) to limit requisite ETL while avoiding aliasing artifacts from tissues located outside the ROI. Shortening the ETL reduces distortion and artifacts within single-shot SE-EPI images and diminishes the T2-filtering effects that can lead to spatial blurring within HASTE images (compared to an equivalent full-FOV acquisition). IVI techniques have been applied during single-shot DW-EPI for diffusion tensor imaging (DTI) of localized brain structure and DTI of the cervical spinal cord [20]. IVI techniques have also been combined with HASTE sequences for real-time abdomino-pelvic imaging [21] and MRI-guided percutaneous biopsy procedures [16,22].

The purpose of our study was to investigate the feasibility of combining the IVI technique with single-shot DW-EPI and DW-SPLICE sequences for renal DWI. To demonstrate the feasibility of the proposed targeted-DWI methods, we compared DWI measurements performed using single-shot DW-SE-EPI, DW-SPLICE, targeted-DW-SE-EPI and targeted-DW-SPLICE methods in both phantoms and normal volunteers.

METHODS

Sequences

The DW-SPLICE pulse sequence was implemented as depicted in Fig. 1A (modified from an existing DW-HASTE sequence). The strong amplitudes and rapid slew rates used for diffusion weighting gradients can produce strong eddy-currents that may cause significant

image distortion. To mitigate these potential eddy-current effects, diffusion sensitivity was obtained with the twice-refocused spin-echo preparation scheme [23]. A HASTE readout strategy was used to for *k*-space acquisition. To avoid the formation of non Carr-Purcell-Meiboom-Gill (CPMG) artifacts, the split acquisition of fast spin-echo acquisition (SPLICE) technique was used to separate spin-echo and stimulated-echo families in each readout direction by doubling the acquisition period using imbalanced readout gradients. Magnetization, in the transverse plane will thus experience an odd or even number of inter-refocusing pulse periods, added coherently to form odd-parity (E1) echoes and even-parity echoes (E2). Magnitude images were reconstructed using E1 and E2 dataset respectively and averaged to form the final image.

The IVI approach was integrated with both the standard DW-SE-EPI sequence and DW-SPLICE sequence (described above) to permit targeted reduced-FOV acquisitions (Fig. 1B) and subsequent comparisons between these methods. For both sequences, the slice-selective gradient for spatially selective RF excitation was applied along the PE direction for the 90o excitation RF pulse and along the slice-selective direction for the 180o refocusing RF pulses. The perpendicular orientation of the slice-selective gradients limited the FOV along the PE direction with signal generated only within the overlapping central region. The PE FOV was controlled by adjusting the amplitude of the slice-selective gradient for the 90o RF pulse while keeping the bandwidth of the 90o RF pulse and the slice thickness of the refocusing RF pulse unchanged. The IVI technique allowed for a reduction of the field of view (FOV) along the PE direction, hence reducing requisite PE steps and shortening the echo train length for both DW-SE-EPI and DW-SPLICE sequences.

All phantom and volunteer studies were performed using a 1.5T clinical MRI scanner (Magnetom Espree, Siemens Medical Solutions, Erlangen, Germany). The imaging parameters for single-shot DW-SE-EPI, DW-SPLICE, targeted-DW-SE-EPI and targeted-DW-SPLICE are shown in Table 1.

Phantom Studies

To demonstrate the efficacy of the IVI technique, we performed a study using a quality control phantom that included resolution grids oriented along both anterior-posterior and left-right directions (marker spacings of 5, 3, 2, 1 and 0.5 mm). A 4-channel head coil with 4 active coil elements was used for signal reception. Images were acquired using single-shot DW-SE-EPI, DW-SPLICE, targeted-DW-SE-EPI and targeted-DW-SPLICE with PE applied along anterior-posterior direction at $b = 0$ sec/mm^2. The FOV for full-FOV and targeted acquisition were 200×200 mm^2 and 125×75 mm^2 respectively.

Next, another phantom study was performed using two bottles containing distilled water and ethanol to compare the ADC values measured using single-shot DW-SE-EPI, DW-SPLICE, targeted-DW-SE-EPI and targeted-DW-SPLICE. Separate images were acquired with 5 *b*-values: 0, 100, 200, 300 and 500 sec/mm^2. ADC maps were reconstructed off-line based upon the slope of the least-square fit line to function: $ADC \cdot b = -\ln(S(b)/S(0))$, where $S(b)$ is the signal intensity measured for images acquired at specific *b*-values. The mean and standard deviation of the ADC values were measured within ROI drawn in each ADC map.

Volunteer Studies

Ten healthy volunteers were enrolled. The study was approved by our Institutional Review Board and informed consent was obtained from all volunteers. A body matrix array coil and spinal array with 5 active coil elements were used for signal reception. Axial and coronal TSE images were acquired for kidney localization. Renal DWI was performed using single-shot DW-SE-EPI, DW-SPLICE, targeted-DW-SE-EPI and targeted-DW-SPLICE sequences,

respectively, with the following *b*-values used for each acquisition: 0, 50, 100, 150, 200, 250, 300, 400, and 500 sec/mm^2. The diffusion gradients were applied in three orthogonal directions and subsequently averaged to minimize the effects of diffusion anisotropy. Nonselective fat saturation pulse was applied before all the sequences to suppress fat signal. Respiratory triggering was used for image acquisition to reduce respiratory motion artifacts. We first acquired a single-slice coronal single-shot DW-SE-EPI image encompassing both kidneys. Next, DW-SPLICE images were acquired at the same imaging position. The FOVs for full-FOV acquisitions were 400×400 mm^2. Reduced-FOV DW images for the left and right kidneys were then separately acquired using the targeted-DW-SE-EPI and targeted-DW-SPLICE sequences with 220 × 130 mm^2 FOV (identical spatial resolution to full FOV acquisition).

In an additional healthy volunteer, we compared the targeted-DWI methods with single-shot DW-SE-EPI technique with PI acquisition. A PI acceleration factor (iPAT) of 3 was used to produce the similar ETL used in the targeted-DWI techniques. TE was optimized for PI acquisition (TE = 79 ms). All other imaging parameters were the same as single-shot DW-SE-EPI without PI acquisition (Table 1).

Qualitative comparisons were made between images obtained with single-shot DW-SE-EPI, DW-SPLICE, targeted-DW-SE-EPI and targeted-DW-SPLICE to evaluate efficacy of the targeted acquisition techniques for reducing artifacts and spatial blurring. Two experienced radiologists (with >10 years combined experience reading abdominal MRI scans) scored DW images with $b = 0$ sec/mm^2 by consensus, blinded to the particular acquisition strategy. Images were scored based on both the artifact level and image sharpness using a 4-point scoring system with 4 as excellent, 3 as good, 2 as acceptable and 1 as poor. Specifically, for artifact level scores, “4” indicated no apparent artifacts; “3” indicated artifacts present but limited bearing upon interpretation; “2” indicated many artifacts limiting interpretation; “1” indicated severe artifacts obstructing visualization of organs and precluding interpretation. For image sharpness level scores, “4” indicated excellent definition of all fine anatomic structures; “3” indicated good overall definition of anatomic structures; “2” indicated adequate definition of most anatomic structures sufficient for interpretation; “1” indicated poor definition of structures, blurring precluding visualization of structures for interpretation. The scores for full-FOV single-shot DW-SE-EPI, full-FOV DW-SPLICE, targeted-DW-SE-EPI and targeted-DW-SPLICE were compared using pair-wise Wilcoxon signed rank tests with a significance level of 0.05.

For all methods, voxel-wise ADC maps were reconstructed using the aforementioned method in the phantom study. Next, an intra-voxel incoherent motion (IVIM) model was used to separate signal decay contributions arising from diffusion and microcirculation: $S(b) = S(0)\cdot[(1-f)\cdot\exp(-b\cdot D)+f\cdot\exp(-b\cdot D^*)]$, where f is the perfusion fraction, D is the diffusion parameter representing the pure diffusion and D* is the diffusion parameter arising from microcirculation and perfusion. Voxel-wise signal measurements were fit to the latter model using the Levenberg-Marquardt algorithm.

For images acquired using single-shot DW-SE-EPI, targeted-DW-SE-EPI and targeted-DW-SPLICE, ROIs were placed in the renal cortex and medulla according to DW images acquired with $b = 0$ sec/mm^2. ROIs were then transferred to ADC, D and f parametric maps and mean ADC, f and D measured in the renal cortex and medulla for both kidneys. A paired Student’s *t*-test was used to compare the mean ADC, D and f calculated for DW images acquired using the three methods with significance level of 0.05.

RESULTS

Phantom studies

Full-FOV images for the resolution phantom acquired using single-shot DW-SE-EPI and DW-SPLICE sequences are shown in Fig. 1c(1) and **1c(2)**. Both targeted-DW-SE-EPI and targeted-DW-SPLICE were able to limit the FOV to a small region encompassing the resolution markers within the lower left quadrant of the phantom; no clearly evident wrapping artifacts were observed. The targeted-DW-SE-EPI sequence (Fig. 1c(3)) effectively reduced spatial distortion at the edge of the phantom (arrow). The full-FOV DW-SPLICE image (Fig. 1c(2)) showed strong spatial blurring along the PE direction; this blurring was dramatically reduced in the targeted-DW-SPLICE image (Fig. 1c(4)) due to shorter ETL.

The ADC values of water and ethanol measured by single-shot DW-SE-EPI, DW-SPLICE, targeted-DW-SE-EPI and targeted-DW-SPLICE were shown in Table 2. The ADC values measured with each of the four methods were similar and in agreement with previously published data [24–26].

Volunteer studies

For DW images acquired using the single-shot DW-SE-EPI sequence, susceptibility artifacts and image distortion was observed in 4 of 10 cases in the left kidney and 2 of 10 cases in the right kidney. The targeted-DW-SE-EPI sequence with reduced ETL was less sensitive to the susceptibility gradients caused by field inhomogeneities and poor shimming. Artifacts and distortions were observed in only 2 left and 1 right kidney examples. Although DW-SPLICE effectively removed field inhomogeneity-induced artifacts and distortions, images were generally blurred in the phase-encoding (PE) direction due to the T2-filtering effects with the long ETL. Overall, no artifacts or blurring were observed for images acquired with the targeted-DW-SPLICE sequence. Fig. 2 and Fig. 3 show two representative cases with suboptimal shimming. The shim values were automatically calculated from pre-scan and were not deliberately changed. DW-images with $b = 0$ sec/mm^2 and their corresponded ADC, D and f maps are displayed. In both cases, full-FOV images encompassing both kidneys were acquired using single-shot DW-SE-EPI (Fig. 2c(1) and Fig 3c(1)) and DW-SPLICE (Fig. 2b and Fig 3b) sequences. Targeted DW images for left and right kidneys were acquired separately using targeted-DW-SE-EPI (Fig. 2c(2) and Fig. 3c(2)) and targeted-DW-SPLICE (Fig. 2c(3) and Fig. 3c(3)) sequences. Severe artifacts can be observed on both DW images and ADC maps using single-shot DW-SE-EPI. In the first case (Fig 2), the susceptibility differences between liver tissue and air-filled gastrointestinal (GI) tract induced field gradients and caused image distortion at the edge of the left kidney. Strong chemical-shift artifacts were observed in the second case (Fig. 3) on the left liver due to the poor static field shimming. There were fewer artifacts in the targeted-DW-SE-EPI images, while targeted-DW-SPLICE produced images with no obvious artifacts or distortions.

Qualitative image scores for DW images at $b = 0$ sec/mm^2 acquired with single-shot DW-SE-EPI, DW-SPLICE, targeted-SE-EPI and targeted-DW-SPLICE are shown in Table 3. The targeted-DW-SE-EPI technique significantly reduced image artifacts compared with the conventional single-shot DW-SE-EPI technique. Significant improvements for both artifact level and image sharpness were observed in the DW images acquired with targeted-DW-SPLICE technique.

In one healthy volunteer, DW-images at $b = 0$ sec/mm^2 (Fig. 4a) and the corresponding ADC maps (Fig. 4b) acquired with single-shot DW-SE-EPI without PI (**Group 1**), single-shot DW-SE-EPI using PI with an iPAT of 3 (**Group 2**), DW-SPLICE (**Group 3**), targeted-

DW-SE-EPI (**Group 4**) and targeted-DW-SPLICE are shown in Fig. 4. Severe distortions and chemical shift artifacts (**arrows in** Fig. 4b(1)) were observed in the DW image acquired with single-shot DW-SE-EPI without PI. Single-shot DW-SE-EPI with iPAT of 3, targeted-DW-SE-EPI and targeted-DW-SPLICE effectively reduced artifacts and distortions and produced DW-images and ADC maps with of similar quality.

The mean ADC, D and f in the renal cortex and medulla measured using single-shot DW-SE-EPI, targeted-DW-SE-EPI and targeted-DW-SPLICE sequences are shown in Table 2–4. For both kidneys, there were no statistically significant differences between the diffusion parameters measured using the three methods ($p > 0.05$). Also, for each method, ADC, D and f measurements were each significantly higher in the cortex than in the medulla ($p < 0.05$ for each comparison). These results were consistent with previously reported literature values [3,6].

DISCUSSION

With phantom and volunteer studies we demonstrated the feasibility of combining targeted acquisition techniques with both DW-SE-EPI and DW-SPLICE sequences to either reduce artifacts and distortion caused by susceptibility differences and poor field shimming or limit spatial blurring due to T2-decay. Compared with conventional single-shot DW-SE-EPI techniques, targeted-DWI methods generally produced images of superior quality. Targeted-DWI sequences produced comparable parametric diffusion measurements to those produced using conventional full FOV single-shot DW-SE-EPI methods.

For these normal volunteer studies, we found that the measured ADC values, largely dependent upon the glomerular filtration rate [6], were significantly higher in the renal cortex than in the medulla. Perfusion fraction f measurements, representing the contribution of microcirculation of blood to the signal decay in the voxel, could potentially serve as a biomarker for perfusion but these do not directly correspond to absolution perfusion measurements. The perfusion fraction was significantly higher in the renal cortex than the value obtained in the renal medulla, likely corresponding to the substantially higher regional blood flow in the renal cortex, which hence may make more contributions to the signal decay. These findings were in accordance with previous studies. [3,6,27]

Single-shot DW-SE-EPI is the most commonly used technique for abdominal DWI due to its relative immunity to bulk motion artifacts. However, severe image artifacts and distortion caused by susceptibility differences and poor static field shimming can limit its application for abdominal imaging. Artifacts and distortion can significantly degrade image quality during renal DWI, particularly for the left kidney adjacent to the GI tract. Alternative fast spin-echo based acquisition techniques, such as DW-PROPELLER[17], DIFRAD-FSE (DW radial acquisition of data with fast spin-echo) [13] or DW-HASTE, can be useful to improve image quality for DWI in kidneys. However, both DW-PROPELLLER and DIFRAD-FSE are multiple-shot approaches requiring longer scan times; increased acquisition duration can be problematic for clinical translation particularly for IVIM or diffusion tensor measurements that require repeated acquisition of DW images (across a potentially wide range of *b*-values or DW orientations). DW-HASTE is single-shot approach that has been applied for DWI in the brain [28–30]; DW-HASTE methods are relatively insensitive to bulk motion, chemical shift artifacts and susceptibility gradients. However, the CPMG condition, which requires the initial transverse magnetization to align with the axis of the refocusing pulses, is violated due to the random phase error accumulated during the diffusion preparation. In order to address this problem, we can ensure that the refocusing flip angle is exactly 180o [31], eliminate the non-CPMG component with additional gradients and RF pulses [29,32], split the acquisition into two components by doubling the receiver bandwidth

(SPLICE) [9] or use quadratic phase modulation for the refocusing RF pulses [30,33]. The first method is not practical due to the non-uniform slice profile across the excitation slice. The second and third methods reduce the SNR by factors of 2 and compared to standard fast spin-echo acquisitions. Although quadratic phase modulation of the refocusing RF pulses can preserve the full signal without attenuation, the same PE line has to be acquired twice in order to separate real and imaginary components of the transverse magnetization for image reconstruction thus doubling ETL leading to spatial blurring due to T2-decay. To achieve the compromises between SNR and ETL, SPLICE was chosen to avoid the CPMG artifacts for DW-HASTE acquisitions during this current study.

We have demonstrated that artifact levels in the single-shot DW-SE-EPI images and spatial blurring in the DW-SPLICE images can be reduced by shortening the ETL. In this work, we applied the targeted acquisition approach with single-shot DW-SE-EPI as well as DW-SPLICE to reduce ETL (roughly 40% of original ETL) and limit the PE FOV in both phantom and volunteer studies. As expected, compared with full-FOV image acquisitions, targeted-DW-SE-EPI successfully reduced distortion in the areas with large susceptibility differences, while targeted-DW-SPLICE effectively reduced spatial blurring and increased the observable spatial resolution. When comparing between targeted-DW-SE-EPI and targeted-DW-SPLICE techniques, qualitative evaluations in volunteer studies demonstrated that the targeted-DW-SPLICE method produced superior image quality based on artifact level and image sharpness scores. Targeted-DW-SPLICE images displayed superior definition of anatomical structures and fewer artifacts, particularly in regions with large susceptibility differences or suboptimal shimming where DW-EPI techniques tended to fail; targeted-DW-SPLICE is a TSE-based imaging sequence and hence intrinsically less sensitive to field inhomogeneities and chemical shift artifacts. PI acquisition techniques, such as SENSE [34] and GRAPPA [35], can be applied during single-shot DW-SE-EPI for ETL reduction. In our study, targeted-DWI techniques were compared with single-shot DW-SE-EPI using PI with an iPAT = 3 in a healthy volunteer. We found that single-shot DW-SE-EPI, targeted-SE-EPI and targeted-DW-SPLICE techniques effectively reduced artifacts and distortions observed in the DW images acquired with single-shot DW-SE-EPI without PI acquisition. In contrast to PI methods, which reduce ETL depending on the coil geometry, targeted image acquisition techniques reduce ETL with a dependence only upon the ratio of the desired FOV to the full FOV. PI methods could potentially also be utilized during these targeted-DWI acquisitions to further reduce ETL. 2D spatially selective echo-planar RF excitation[15,36] and outer volume suppression [20,37] techniques have been used for targeted reduced FOV DWI in the spinal cord and brain. However, to achieve a sharp slice excitation profile the requisite duration of 2DRF pulses is relatively long typically leading to increases in echo times and thus T2-related signal losses. OVS techniques are typically quite sensitive to B_1 inhomogeneities and resulting images can suffer from aliasing artifacts due to T1 recovery within OV regions.

Targeted-DWI approaches have several limitations. For these studies targeted acquisition provided superior overall image quality at the expense of in-plane spatial coverage. Targeted-DW images for the left and right kidneys were acquired separately due to the limited FOV, which doubled the imaging time. Furthermore, the perpendicular direction of the slice-selective gradients for the 90o excitation RF pulses and 180o refocusing RF pulses will complicate multiple slice image acquisition. Depending upon the excitation RF flip angle and tissue T1 relaxation, interleaved slice acquisition to accelerate volumetric coverage may be difficult due to insufficient longitudinal magnetization recovery between excitations. The value of the presented single-slice DWI techniques for clinical application may be minimal if the limitation of requiring a single slice acquisition cannot be overcome. Wheeler-Kingshott et al. [38] developed a modified IVI technique: the zonal oblique multi-slice (ZOOM) method that involves applying an oblique 180o refocusing pulse, rather than

an orthogonal pulse. This approach makes interleaved multiple slice acquisition possible by setting a suitable gap between slices. Future studies could incorporate ZOOM techniques to improve multi-slice imaging efficiency for targeted single-shot DW-SE-EPI and DW-SPLICE sequences. Another limitation of this study was that the SNR characteristics for these different acquisition strategies were not rigorously compared. For the targeted acquisitions with a majority of the FOV containing tissue signals, conventionally calculated SNR values (i.e. those based upon noise estimates from peripheral regions of air void of tissue) were not readily obtainable; however, we would anticipate a theoretical SNR reduction of roughly 44% compared to a full *k*-space, given that SNR is proportional to the square root of the product of the number of readout samples and the number of phase-encoding samples for a given slice. Moreover, for each acquisition, the shim values were calculated only once for each slice position based upon automated pre-scan adjustment and tuning procedures; peristalsis within the GI tract could lead to changes in local field inhomogeneities that may not have been optimally compensated due to the use of only the initially calculated pre-scan shim values. The latter conditions could have differentially impacted image quality during the separate full FOV and targeted acquisitions.

In conclusion, we have demonstrated the feasibility of combining the targeted acquisition IVI technique with single-shot DW-SE-EPI and DW-SPLICE for renal DW and IVIM measurements. Compared with full-FOV DW imaging, targeted-DW-SE-EPI and targeted-DW-SPLICE techniques reduced image distortion and artifacts observed in the single-shot DW-SE-EPI images, reduced blurring in DW-SPLICE images and produced comparable quantitative DW and IVIM measurements to those produced with conventional full-FOV approaches.

References

1. Le Bihan D, Breton E, Lallemand D, Aubin ML, Vignaud J, Laval-Jeantet M. Separation of diffusion and perfusion in intravoxel incoherent motion MR imaging. Radiology. 1988; 168(2):497–505. [PubMed: 3393671]
2. Turner R, Le Bihan D, Maier J, Vavrek R, Hedges LK, Pekar J. Echo-planar imaging of intravoxel incoherent motion. Radiology. 1990; 177(2):407–414. [PubMed: 2217777]
3. Thoeny HC, De Keyzer F, Oyen RH, Peeters RR. Diffusion-weighted MR imaging of kidneys in healthy volunteers and patients with parenchymal diseases: initial experience. Radiology. 2005; 235(3):911–917. [PubMed: 15845792]
4. Namimoto T, Yamashita Y, Mitsuzaki K, Nakayama Y, Tang Y, Takahashi M. Measurement of the apparent diffusion coefficient in diffuse renal disease by diffusion-weighted echo-planar MR imaging. J Magn Reson Imaging. 1999; 9(6):832–837. [PubMed: 10373031]
5. Muller MF, Prasad PV, Bimmler D, Kaiser A, Edelman RR. Functional imaging of the kidney by means of measurement of the apparent diffusion coefficient. Radiology. 1994; 193(3):711–715. [PubMed: 7972811]
6. Thoeny HC, Zumstein D, Simon-Zoula S, et al. Functional evaluation of transplanted kidneys with diffusion-weighted and BOLD MR imaging: initial experience. Radiology. 2006; 241(3):812–821. [PubMed: 17114628]
7. Zhang J, Tehrani YM, Wang L, Ishill NM, Schwartz LH, Hricak H. Renal masses: characterization with diffusion-weighted MR imaging--a preliminary experience. Radiology. 2008; 247(2):458–464. [PubMed: 18430878]
8. Farzaneh F, Riederer SJ, Pelc NJ. Analysis of T2 limitations and off-resonance effects on spatial resolution and artifacts in echo-planar imaging. Magn Reson Med. 1990; 14(1):123–139. [PubMed: 2352469]
9. Schick F. SPLICE: sub-second diffusion-sensitive MR imaging using a modified fast spin-echo acquisition mode. Magn Reson Med. 1997; 38(4):638–644. [PubMed: 9324331]
10. Bammer R, Auer M, Keeling SL, et al. Diffusion tensor imaging using single-shot SENSE-EPI. Magn Reson Med. 2002; 48(1):128–136. [PubMed: 12111940]

11. Taouli B, Martin AJ, Qayyum A, et al. Parallel imaging and diffusion tensor imaging for diffusion-weighted MRI of the liver: preliminary experience in healthy volunteers. AJR Am J Roentgenol. 2004; 183(3):677–680. [PubMed: 15333355]
12. Butts K, de Crespigny A, Pauly JM, Moseley M. Diffusion-weighted interleaved echo-planar imaging with a pair of orthogonal navigator echoes. Magn Reson Med. 1996; 35(5):763–770. [PubMed: 8722828]
13. Trouard TP, Theilmann RJ, Altbach MI, Gmitro AF. High-resolution diffusion imaging with DIFRAD-FSE (diffusion-weighted radial acquisition of data with fast spin-echo) MRI. Magn Reson Med. 1999; 42(1):11–18. [PubMed: 10398944]
14. Pipe JG, Farthing VG, Forbes KP. Multishot diffusion-weighted FSE using PROPELLER MRI. Magn Reson Med. 2002; 47(1):42–52. [PubMed: 11754441]
15. Saritas EU, Cunningham CH, Lee JH, Han ET, Nishimura DG. DWI of the spinal cord with reduced FOV single-shot EPI. Magn Reson Med. 2008; 60(2):468–473. [PubMed: 18666126]
16. Zimmermann H, Muller S, Gutmann B, et al. Targeted-HASTE imaging with automated device tracking for MR-guided needle interventions in closed-bore MR systems. Magn Reson Med. 2006; 56(3):481–488. [PubMed: 16795081]
17. Deng J, Miller FH, Salem R, Omary RA, Larson AC. Multishot diffusion-weighted PROPELLER magnetic resonance imaging of the abdomen. Invest Radiol. 2006; 41(10):769–775. [PubMed: 16971801]
18. Einarsdottir H, Karlsson M, Wejde J, Bauer HC. Diffusion-weighted MRI of soft tissue tumours. Eur Radiol. 2004; 14(6):959–963. [PubMed: 14767604]
19. Feinberg DA, Hoenninger JC, Crooks LE, Kaufman L, Watts JC, Arakawa M. Inner volume MR imaging: technical concepts and their application. Radiology. 1985; 156(3):743–747. [PubMed: 4023236]
20. Jeong EK, Kim SE, Guo J, Kholmovski EG, Parker DL. High-resolution DTI with 2D interleaved multislice reduced FOV single-shot diffusion-weighted EPI (2D ss-rFOV-DWEPI). Magn Reson Med. 2005; 54(6):1575–1579. [PubMed: 16254946]
21. Makki M, Graves MJ, Lomas DJ. Interactive body magnetic resonance fluoroscopy using modified single-shot half-Fourier rapid acquisition with relaxation enhancement (RARE) with multiparameter control. J Magn Reson Imaging. 2002; 16(1):85–93. [PubMed: 12112507]
22. Buecker A, Adam G, Neuerburg JM, Glowinski A, van Vaals JJ, Guenther RW. MR-guided biopsy using a T2-weighted single-shot zoom imaging sequence (Local Look technique). J Magn Reson Imaging. 1998; 8(4):955–959. [PubMed: 9702898]
23. Reese TG, Heid O, Weisskoff RM, Wedeen VJ. Reduction of eddy-current-induced distortion in diffusion MRI using a twice-refocused spin echo. Magn Reson Med. 2003; 49(1):177–182. [PubMed: 12509835]
24. Niendorf T, Norris DG, Leibfritz D. Detection of apparent restricted diffusion in healthy rat brain at short diffusion times. Magn Reson Med. 1994; 32(5):672–677. [PubMed: 7808271]
25. Toft PB, Leth H, Peitersen B, Lou HC, Thomsen C. The apparent diffusion coefficient of water in gray and white matter of the infant brain. J Comput Assist Tomogr. 1996; 20(6):1006–1011. [PubMed: 8933811]
26. Tofts PS, Lloyd D, Clark CA, et al. Test liquids for quantitative MRI measurements of self-diffusion coefficient in vivo. Magn Reson Med. 2000; 43(3):368–374. [PubMed: 10725879]
27. Ries M, Jones RA, Basseau F, Moonen CT, Grenier N. Diffusion tensor MRI of the human kidney. J Magn Reson Imaging. 2001; 14(1):42–49. [PubMed: 11436213]
28. Nolte UG, Finsterbusch J, Frahm J. Rapid isotropic diffusion mapping without susceptibility artifacts: whole brain studies using diffusion-weighted single-shot STEAM MR imaging. Magn Reson Med. 2000; 44(5):731–736. [PubMed: 11064408]
29. Alsop DC. Phase insensitive preparation of single-shot RARE: application to diffusion imaging in humans. Magn Reson Med. 1997; 38(4):527–533. [PubMed: 9324317]
30. Bastin ME, Le Roux P. On the application of a non-CPMG single-shot fast spin-echo sequence to diffusion tensor MRI of the human brain. Magn Reson Med. 2002; 48(1):6–14. [PubMed: 12111926]

31. Beaulieu CF, Zhou X, Cofer GP, Johnson GA. Diffusion-weighted MR microscopy with fast spin-echo. Magn Reson Med. 1993; 30(2):201–206. [PubMed: 8366801]
32. Norris DG, Bornert P, Reese T, Leibfritz D. On the application of ultra-fast RARE experiments. Magn Reson Med. 1992; 27(1):142–164. [PubMed: 1435200]
33. Le Roux P. Non-CPMG Fast Spin Echo with full signal. J Magn Reson. 2002; 155(2):278–292. [PubMed: 12036339]
34. Pruessmann KP, Weiger M, Scheidegger MB, Boesiger P. SENSE: sensitivity encoding for fast MRI. Magn Reson Med. 1999; 42(5):952–962. [PubMed: 10542355]
35. Griswold MA, Jakob PM, Heidemann RM, et al. Generalized autocalibrating partially parallel acquisitions (GRAPPA). Magn Reson Med. 2002; 47(6):1202–1210. [PubMed: 12111967]
36. Finsterbusch J. High-resolution diffusion tensor imaging with inner field-of-view EPI. J Magn Reson Imaging. 2009; 29(4):987–993. [PubMed: 19306448]
37. Wilm BJ, Svensson J, Henning A, Pruessmann KP, Boesiger P, Kollias SS. Reduced field-of-view MRI using outer volume suppression for spinal cord diffusion imaging. Magn Reson Med. 2007; 57(3):625–630. [PubMed: 17326167]
38. Wheeler-Kingshott CA, Parker GJ, Symms MR, et al. ADC mapping of the human optic nerve: increased resolution, coverage, and reliability with CSF-suppressed ZOOM-EPI. Magn Reson Med. 2002; 47(1):24–31. [PubMed: 11754439]

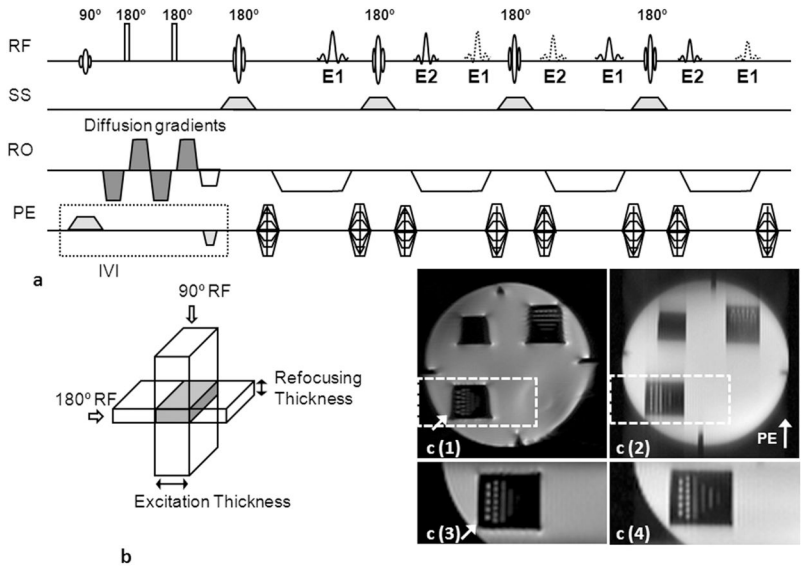

Figure 1.

(**a**) Targeted-DW-SPLICE pulse sequence diagram, (**b**) IVI scheme. To avoid non-CPMG artifacts, the spin echoes (solid lines) and stimulated echoes (dash lines) were separated by doubling the readout gradient durations. Odd (E1) and even (E2) echoes were formed alternatively into spin and stimulated echoes. Magnitude images were reconstructed using E1 and E2 datasets respectively; these were subsequently averaged to form the final image. The slice-selective gradient for the 90o excitation pulse is applied along the PE direction, while the slice-selective gradient for the180o refocusing pulses are applied along the slice-selective direction to provide a limited FOV along the PE direction. Signal formation is limited to the overlapping region between the two selective excitation pulses (gray region in **b**). (c) Images of the resolution phantom acquired using full FOV single-shot DW-SE-EPI (**c(1)**) and full FOV DW-SPLICE (**c(2)**) sequences; reduced FOV images covering the resolution markers within the lower left quadrant of the phantom (dash boxes in **c(1)** and **c(2)**) acquired using targeted-DW-SE-EPI (**c(3)**) and targeted-DW-SPLICE (**c(4)**). Less image distortion (arrow in **c(1)**) was observed in targeted-DW-SE-EPI image. The targeted-DW-SPLICE sequence effectively reduced blurring in the PE direction compared to full-FOV DW-SPLICE.

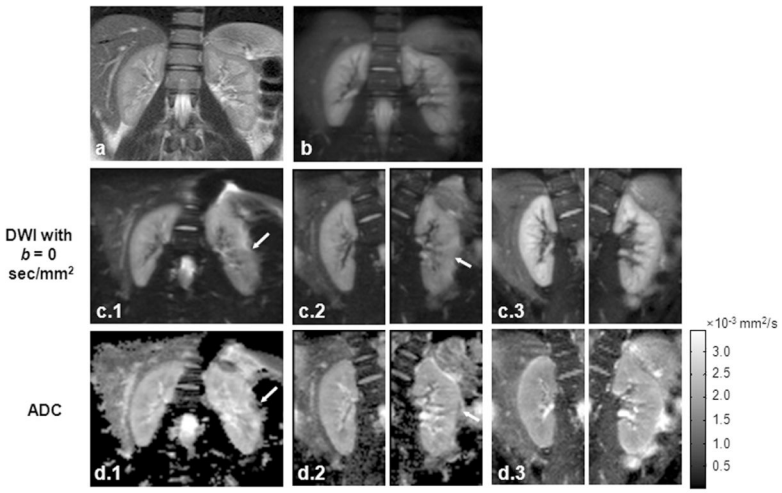

Figure 2.

First representative *in vivo* example: (**a**) coronal TSE localization image, (**b**) full-FOV DW-SPLICE image at b = 0 sec/mm^2, (**c**-**d**) DW images at b = 0 sec/mm^2 (**c**) and their corresponding ADC (**d**) maps acquired using single-shot DW-SE-EPI (**Group 1**), targeted-DW-SE-EPI (**Group 2**) and targeted-DW-SPLICE (**Group 3**). Spatial distortion is observed at the edge of the left kidney in both single-shot DW-SE-EPI and targeted-DW-SE-EPI images due to susceptibility-induced field gradient adjacent to air-filled GI tract (arrows within **c** and **d**).

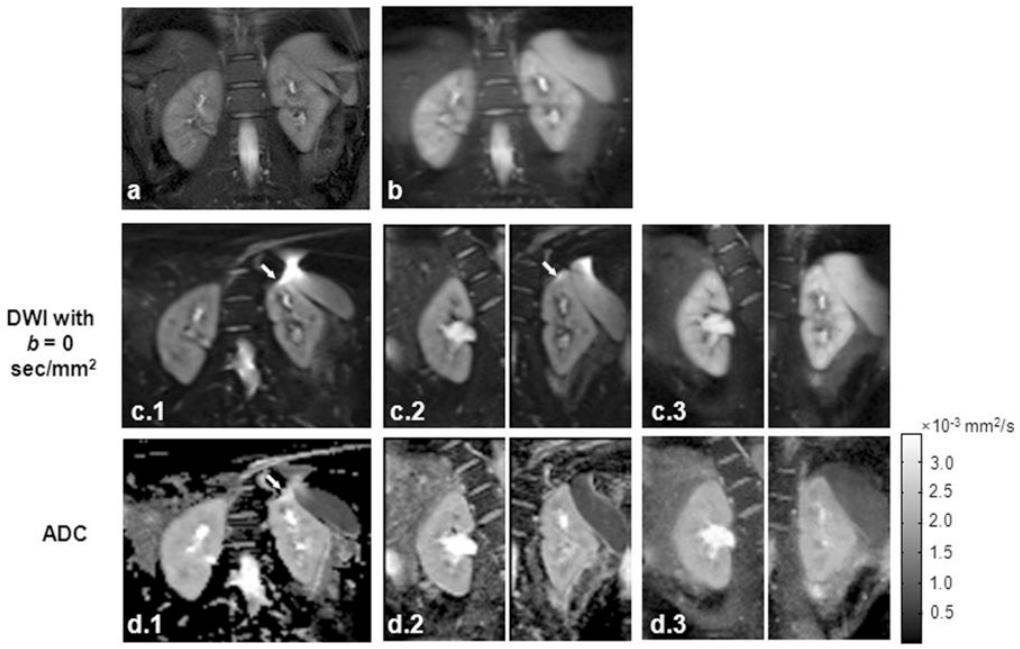

Figure 3.

Second representative *in vivo* example: (**a**) coronal TSE localization image, (**b**) full-FOV DW-SPLICE image at b = 0 sec/mm^2, (**c–d**) DW images at b = 0 sec/mm^2 (**c**) and their corresponding ADC (**d**) maps acquired using single-shot DW-SE-EPI (**Group 1**), targeted-DW-SE-EPI (**Group 2**) and targeted-DW-SPLICE (**Group 3**). Chemical-shift artifacts are observed within the left kidney for both single-shot DW-SE-EPI and targeted-DW-SE-EPI images (arrows in **c** and **d**).

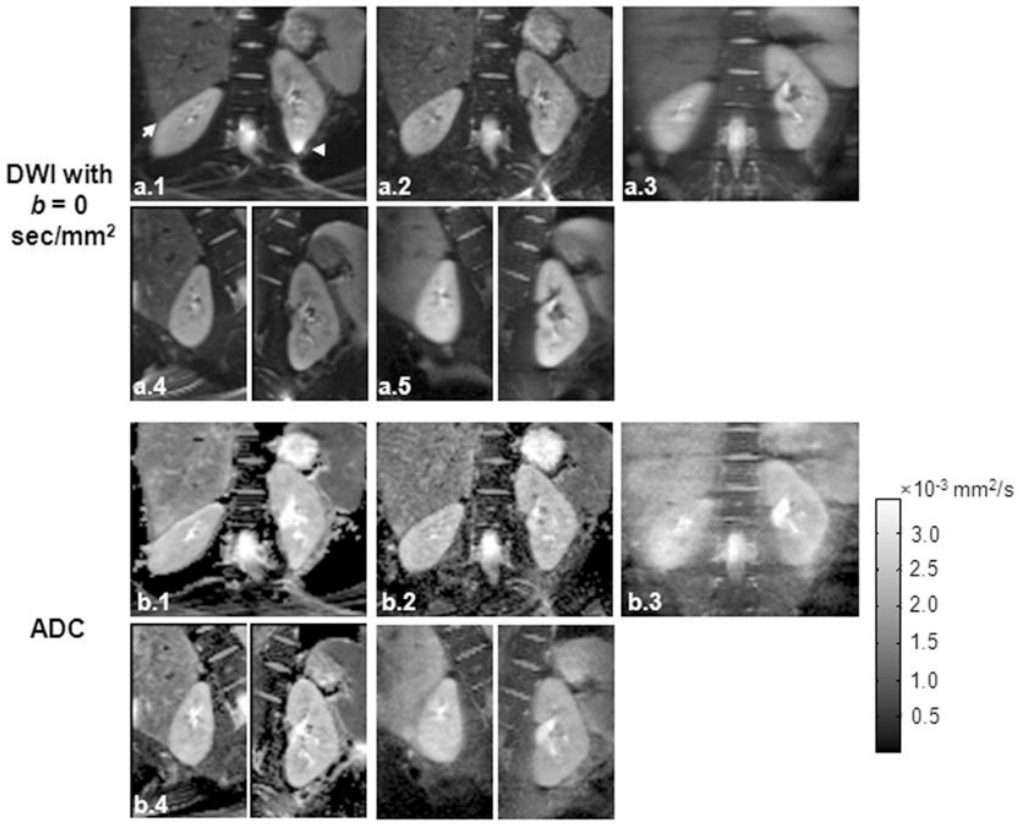

Figure 4.

Comparisons between targeted-DWI and single-shot DW-SE-EPI with PI acquisition in a healthy volunteer: (**a**) DW images at b = 0 sec/mm^2 and (**b**) the corresponding ADC maps acquired using single-shot DW-SE-EPI without PI (**Group 1**), single-shot DW-SE-EPI using PI with an iPAT of 3 (**Group 2**), DW-SPLICE (**Group 3**), targeted-DW-SE-EPI (**Group 4**) and targeted-DW-SPLICE (Group 5). Distortion and artifacts are clearly observed within the single-shot DW-SE-EPI image (arrows in **a(1)**).

Table 1

Imaging parameters for single-shot DW-SE-EPI, DW-SPLICE, targeted-DW-SE-EPI and targeted-DW-SPLICE sequences

	Single-shot DW-SE-EPI	DW-SPLICE	Targeted DW-SE-EPI	Targeted DW-SPLICE
TR/TE (ms)	97/3000	57/3000	81/3000	57/3000
TH (mm)	5	5	5	5
Matrix	128×128	128×128	80×48	80×48
BW (Hz/Pixel)	1500	800	1500	800
Echo Spacing for phantom Studies(ms)	1.02	4.02	1.01	4.04
Echo Spacing for Volunteer Studies(ms)	0.73	3.86	0.74	3.88
ETL	84	72	32	32
Signal Averages	3	3	3	3
Fat Saturation	Yes	Yes	Yes	Yes

Table 2

ADC values of water and ethanol measured with single-shot DW-SE-EPI, DW-SPLICE, targeted-DW-SE-EPI and targeted-DW-SPLICE techniques

ADC ($\times 10^{-3}$ mm^2/s)	Single-shot DW-SE-EPI	DW-SPLICE	Targeted-DW-SE-EPI	Targeted-DW-SPLICE	Literature[24–26]
Water	2.16±0.05	2.18±0.05	2.15±0.03	2.17±0.05	2.0–2.5
Ethanol	1.04±0.2	1.08±0.3	1.05±0.15	1.11±0.2	1.0–1.2

Table 3

Qualitative image scores for DW-images at $b = 0$ sec/mm^2 acquired with single-shot DW-SE-EPI, DW-SPLICE, targeted-DW-SE-EPI and targeted-DW-SPLICE techniques

Image Score	Single-shot DW-SE-EPI	DW-SPLICE	Targeted-DW-SE-EPI	Targeted-DW-SPLICE
Artifacts	$1.56 \pm 0.53^{\dagger *\ddagger}$	$2.89 \pm 0.6^{\dagger}$	$2.89 \pm 0.78^{\dagger}$	3.67 ± 0.5
Sharpness	$2.89 \pm 0.33^{\dagger\ddagger}$	$2.22 \pm 0.33^{\dagger}$	$2.89 \pm 0.33^{\dagger\ddagger}$	3.67 ± 0.5

$^{\dagger}p < 0.05$ for comparisons with qualitative image score for DW-images acquired by targeted-DW-SPLICE

$^{*}p < 0.05$ for comparisons with qualitative image score for DW-images acquired by targeted-DW-SE-EPI

$^{\ddagger}p < 0.05$ for comparisons with qualitative image score for DW-images acquired by DW-SPLICE

Table 4

Mean ADC, f and D in the cortex and medulla for both left and right kidneys measured using single-shot DW-SE-EPI, DW-SPLICE, targeted-DW-SE-EPI and targeted-DW-SPLICE sequences

		ADC ($\times 10^{-3}$ mm^2/s)*		f*		D ($\times 10^{-3}$ mm^2/s)*	
		Cortex	**Medulla**	**Cortex**	**Medulla**	**Cortex**	**Medulla**
Left	Single-shot DW-SE-EPI	2.37±0.13	2.18±0.08	0.18±0.02	0.16±0.05	2.03±0.24	1.88±0.18
	Targeted-SE-EPI	2.32±0.10	2.14±0.09	0.18±0.03	0.16±0.03	1.95±0.22	1.84±0.24
	Targeted-DW-SPLICE	2.33±0.13	2.13±0.10	0.19±0.02	0.17±0.02	1.85±0.22	1.77±0.21
Right	Single-shot DW-SE-EPI	2.36±0.13	2.15±0.11	0.20±0.03	0.17±0.03	1.96±0.16	1.85±0.16
	Targeted-SE-EPI	2.29±0.13	2.10±0.10	0.19±0.03	0.16±0.03	1.96±0.16	1.77±0.06
	Targeted-DW-SPLICE	2.32±0.13	2.12±0.11	0.20±0.03	0.18±0.03	1.88±0.12	1.78±0.08

* Data are mean ± standard deviations.